Computers in Biology and Medicine 133 (2021) 104287

Contents lists available at ScienceDirect

Computers in Biology and Medicine

journal homepage: www.elsevier.com/locate/compbiomed

Automatic detection of generalized paroxysmal fast activity in interictal EEG using time-frequency analysis

Amir Omidvarnia [a,b,*], Aaron E.L. Warren [c,d], Linda J. Dalic [c,d,e], Mangor Pedersen [f], Graeme Jackson [c,e]

[a] Institute of Bioengineering, Center for Neuroprosthetics, Center for Biomedical Imaging, EPFL, Geneva, Switzerland
[b] Department of Radiology and Medical Informatics, University of Geneva, Geneva, Switzerland
[c] The Florey Institute of Neuroscience and Mental Health, Melbourne, Australia
[d] Department of Medicine, Austin Health, The University of Melbourne, Melbourne, Australia
[e] Department of Neurology, Austin Health, Melbourne, Australia
[f] Department of Psychology and Neuroscience, Auckland University of Technology, Auckland, New Zealand

ARTICLE INFO

Keywords:
EEG
fMRI
Epilepsy
Automatic spike detection
Interictal epileptiform discharge
Time-frequency analysis
Lennox-gastaut syndrome
Generalized paroxysmal fast activity
General linear modelling

ABSTRACT

Objective: Markup of generalized interictal epileptiform discharges (IEDs) on EEG is an important step in the diagnosis and characterization of epilepsy. However, manual EEG markup is a time-consuming, subjective, and the specialized task where the human reviewer needs to visually inspect a large amount of data to facilitate accurate clinical decisions. In this study, we aimed to develop a framework for automated detection of generalized paroxysmal fast activity (GPFA), a generalized IED seen in scalp EEG recordings of patients with the severe epilepsy of Lennox-Gastaut syndrome (LGS).

Methods: We studied 13 children with LGS who had GPFA events in their interictal EEG recordings. Time-frequency information derived from manually marked IEDs across multiple EEG channels was used to automatically detect similar events in each patient's interictal EEG. We validated true positives and false positives of the proposed spike detection approach using both standalone scalp EEG and simultaneous EEG-functional MRI (EEG-fMRI) recordings.

Results: GPFA events displayed a consistent low-high frequency arrangement in the time-frequency domain. This 'bimodal' spectral feature was most prominent over frontal EEG channels. Our automatic detection approach using this feature identified EEG events with similar time-frequency properties to the manually marked GPFAs. Brain maps of EEG-fMRI signal change during these automatically detected IEDs were comparable to the EEG-fMRI brain maps derived from manual IED markup.

Conclusion: GPFA events have a characteristic bimodal time-frequency feature that can be automatically detected from scalp EEG recordings in patients with LGS. The validity of this time-frequency feature is demonstrated by EEG-fMRI analysis of automatically detected events, which recapitulates the brain maps we have previously shown to underlie generalized IEDs in LGS.

Significance: This study provides a novel methodology that enables a fast, automated, and objective inspection of generalized IEDs in LGS. The proposed framework may be extendable to a wider range of epilepsy syndromes in which monitoring the burden of epileptic activity can aid clinical decision-making and faster assessment of treatment response and estimation of future seizure risk.

1. Introduction

Generalized interictal epileptiform discharges (IEDs) are a characteristic feature of the interictal (i.e., 'between seizures') scalp electroencephalogram (EEG) in multiple forms of epilepsy. Generalized IEDs are typically seen across bilaterally distributed scalp electrodes and show a time-varying morphology. The precise temporo-spatial appearance of these IEDs depends on the extent and location of the underlying

* Corresponding author. Medical Image Processing lab, Campus Biotech, Chemin des Mines 9, 1202, Geneva, Switzerland.
E-mail addresses: amir.omidvarnia@epfl.ch (A. Omidvarnia), aaron.warren@unimelb.edu.au (A.E.L. Warren), linda.dalic@austin.org.au (L.J. Dalic), mangor.pedersen@florey.edu.au (M. Pedersen), graeme.jackson@florey.edu.au (G. Jackson).

https://doi.org/10.1016/j.compbiomed.2021.104287
Received 22 October 2020; Received in revised form 12 February 2021; Accepted 13 February 2021
Available online 3 March 2021

Table 1
Demographic and electroclinical information of the children with LGS. For each patient, the total number and cumulative duration (in seconds) is provided for their manually marked GPFA events that were captured during EEG-fMRI scanning.

ID	Age at scan (yr)	Age of seizure onset (yr)	Gender	Etiological type presumed to underlie epilepsy	Anatomical MRI findings	EEG-fMRI study length (min)	No. of manually marked GPFA events (cumulative duration in sec)
S1	10	0.8	F	Structural/genetic	Right medial temporal lobe DNET	30	18 (16.2)
S2	2	1	M	Structural	Left temporal lobe dysplasia	30	106 (92.5)
S3	13	12	F	Unknown	Unremarkable	30	20 (15.5)
S4	13	0.4	F	Unknown	Cerebellar atrophy (incidental)	16	74 (52.3)
S5	5	0	M	Structural/metabolic	Bilateral occipital ulegyria	30	114 (106.8)
S6	11	0.8	F	Infectious/structural	Bilateral encephalomalacia and gliosis involving insula, perisylvian, and prerolandic regions	22	87 (50.2)
S7	12	0.25	F	Genetic/structural	Tuberous sclerosis with multiple cortical tubers	30	60 (64.6)
S8	7	2.5	F	Infectious/structural	Bilateral encephalomalacia involving frontal, temporal, parietal, ad insular cortex, basal ganglia, hippocampus	30	137 (135.3)
S9	15	0.3	M	Unknown	Unremarkable	30	34 (72.8)
S10	6	3	M	Infectious/structural	Bilateral hippocampal sclerosis	30	124 (112.6)
S11	10	2	F	Infectious/structural	Bilateral hippocampal sclerosis	30	45 (73.2)
S12	16	2.7	F	Unknown	Unremarkable with previous left temporal lobe corticectomy	30	43 (29)
S13	4	0.2	F	Genetic	Unremarkable	30	97 (53.9)
Mean $\pm$ ***std***							69 $\pm$ 43 (62 $\pm$ 40)

epileptic brain network. These complex brain dynamics make generalized IEDs challenging to differentiate from 'normal' background activity, even for experienced human reviewers. Characterization of generalized IEDs in the time-frequency domain is a potential method to aid manual markup, and may assist with the development of automatic IED detection approaches.

Lennox-Gastaut syndrome (LGS) is a type of epilepsy where generalized IEDs are frequent. LGS is a severe, childhood-onset epilepsy associated with drug-resistant seizures, characteristic scalp EEG patterns, and disabling cognitive and behavioural impairments that worsen over time [1,2]. The onset of LGS is typically heralded by a plateauing of cognitive development or loss of previously acquired cognitive skills, in part due to the impact of frequent epileptic activity on the developing brain [3,4].

An important characteristic of the interictal EEG in LGS is the existence of generalized paroxysmal fast activity (GPFA) events with a spectral content of ~8–20 Hz. Clinical assessment of these events is usually performed manually by human experts who are required to carefully review each page of EEG over a recording that may last 24 h or more. Although clinically informative, this process is subjective, time-consuming, and often impractical. Due to time constraints, careful manual review of the entire recording is rarely performed, with human reviewers estimating the IED burden from a sub-sample of the entire EEG recording.

There are several automatic IED detection methods in the literature which can be categorized into three groups: time-domain methods, frequency-domain methods and wavelet-domain methods. Short-time Fourier transform, wavelet transforms, empirical mode decomposition, and Fourier decomposition method can be adapted to interrogate epileptiform discharges from different perspectives (see Ref. [5] for a comprehensive review). Machine learning approaches [6,7], phase synchrony analysis [8], time-frequency analysis [9], correlation analysis [10,11], spike morphology-based analysis [12], EEG feature extraction [13–15], sub-band decomposition [16], and independent components analysis [17] have been used for the implementation of the IED detection methods.

Despite a large number of existing automated spike detection techniques, only a small number of commercial software programs are available for real-world applications in epilepsy monitoring units (see,[1,2,3]). However, these programs were developed specifically for the detection of monomorphic *focal* IEDs as opposed to bursts of generalized discharges, which are typically more challenging for automatic detection algorithms due to their highly variable duration and morphology. Hence, these programs are not currently suitable for detection of GPFA in patients with LGS, in whom automated detection is likely to have important clinical benefits. For example, automatic quantification of GPFA burden may provide an objective and complementary measure of treatment response in patients undergoing therapeutic clinical trials [18].

In this study, we investigated EEG signal dynamics of GPFA in the time-frequency domain in a cohort of children with LGS. We showed that GPFA displays a consistent spectral power 'bimodality'. To evaluate the utility of this feature, we searched for segments of patients' EEG recordings with similar time-frequency properties. This was achieved by developing a practical automatic IED detection method based on band-pass filtering of scalp EEG electrodes within two frequency intervals of interest, followed by integration of their instantaneous power envelopes across all scalp electrodes. Reliability of the automatically detected events was evaluated in two ways: (*i*) we assessed true positives by comparing automatically detected GPFA events to the events detected by manual human markup; and (*ii*) we assessed biological plausibility of false positive events (i.e., automatically detected events that were not identified in the manual human markup) by investigating simultaneous EEG-fMRI brain maps derived from manually marked and automatically detected events separately: the key hypothesis here was that if the automatically detected GPFA-like events are biologically meaningful, they should yield EEG-fMRI maps that resemble ones derived from manual human markup of IEDs.

2. Materials and methods

2.1. Patients and simultaneous EEG-fMRI acquisition

Thirteen children with LGS underwent EEG-fMRI at the Royal Children's Hospital in Melbourne, Australia. In all cases, diagnosis of LGS was defined by (*i*) multiple seizure types, including tonic seizures; (*ii*)

[1] http://compumedicsneuroscan.com/curry-epilepsy-evaluation/.
[2] https://www.cadwell.com.
[3] http://www.natus.com.

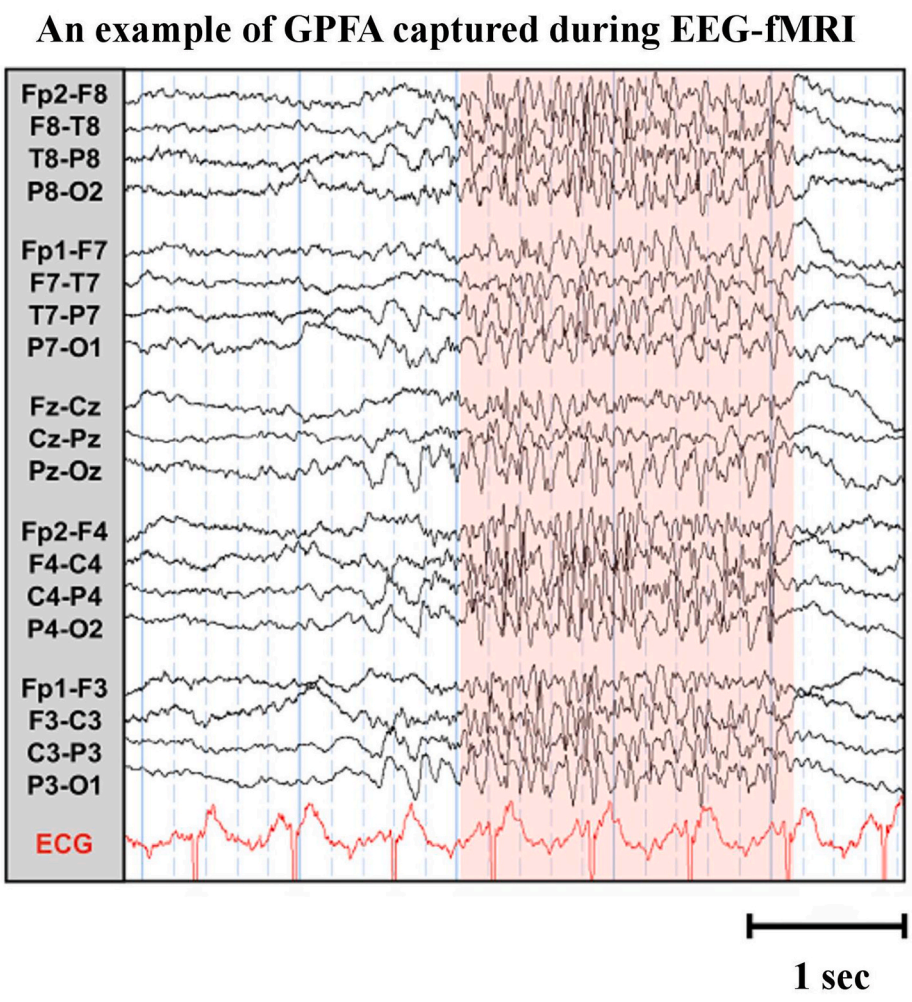

Fig. 1. Example of a multichannel generalized paroxysmal fast activity (GPFA) event captured on the double banana montage during simultaneous EEG-fMRI in a patient with LGS. The Event has been highlighted by a transparent red box. As the highlighted segment illustrates, the morphology, duration and spectral content of the GPFA events at each EEG channel may be different. Also, the events have channel-specific onset times. In other words, GPFA events represent a non-uniform morphology along the time-axis and across EEG channels (i.e., in all temporal, spectral and spatial domains).

routine interictal EEG showing GPFA and bursts of <3 Hz slow spike-and-wave (SSW); and (*iii*) cognitive and/or behavioural impairment [19,20]. The study was approved by the Royal Children's Hospital Human Research Ethics Committee and all parents/legal guardians gave written consent prior to participation. Patients' EEG-fMRI results derived from manual EEG markup are reported in Ref. [20]. Their electroclinical details are summarized in Table 1.

Due to intellectual disability, 12 of the 13 patients were scanned under general anaesthesia (inhalational isoflurane ≤0.8% end-tidal concentration combined with IV remifentanil ≤0.1 μg/kg/min); the remaining patient (S12 in Table 1) tolerated scanning without any anaesthetic agents. FMRI data were acquired in a 3 T S Trio system (Munich, Germany) using an echo-planar imaging sequence with 44 interleaved slices [no gap], repetition time = 3.2 s, echo time = 40 msec and voxel size = 3.4 × 3.4 × 3.4 mm. For each patient, up to 30 min of fMRI was acquired (mean = 28 min). A high-resolution (0.9 mm^3) T_1-weighted magnetisation-prepared-rapid-gradient-echo (MPRAGE) anatomical brain image was also acquired during each session. Concurrent EEG data were acquired using a commercial 64-channel MR-compatible EEG system (Compumedics Neuroscan, Victoria, Australia) according to the 10–20 standard system. Data were recorded based on the referential montage at the sampling rate of 5000 Hz.

2.1.1. Manual markup of generalized IEDs

Each patient's in-scanner EEG was marked by an epileptologist for multiple IED types including GPFA. Table 1 summarizes the total number and cumulative duration of the GPFA event type for patients. An in-scanner example of GPFA is shown in Fig. 1.

2.2. EEG-fMRI preprocessing

FMRI data pre-processing followed our prior work [20]. Briefly, each patient's data was corrected for slice-timing and head motion and then spatially smoothed using a Gaussian filter with full-width at half maximum of 6 mm.

EEG recordings were pre-processed using Compumedics Profusion software[4] version 4.0 and the EEGLAB toolbox[5] [21]. Gradient-switching and cardioballistic artefacts were corrected using average artefact template subtraction methods. To avoid computational limitations, the pre-processed EEG recordings were down-sampled to 100 Hz for further analysis.

2.3. Time-frequency characterization of GPFA

To quantify the time-varying properties of the manually marked GPFA events, we transferred them to the time-frequency domain to reveal their joint temporal and spectral characteristics: this step was performed because the morphology of a GPFA event evolves over both time and space (i.e., scalp EEG electrodes). Additionally, its oscillations may slow down or become faster over the course of an individual discharge. Therefore, an appropriate quantitative detection feature for GPFA must take three factors into account: (*i*) variable morphology, (*ii*) time-varying spectral content before and after the event onset, and (*iii*)

[4] https://www.compumedics.com.au/products/profusion-eeg.
[5] https://sccn.ucsd.edu/eeglab/index.php.

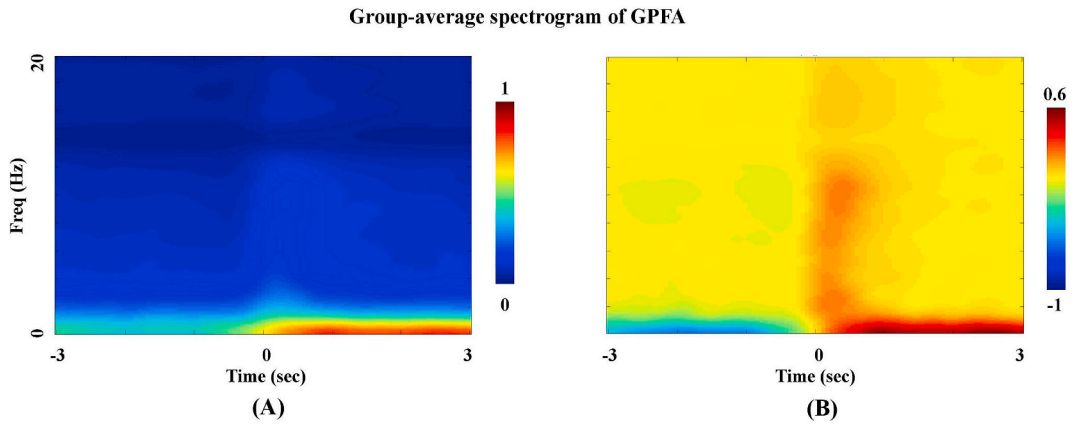

Fig. 2. Group average time-frequency representations of GPFA events calculated in the period from 3 s before to 3 s after the onset of manually marked events over (A) all events and all LGS patients (N = 13), (B) the same events and patients as (A), but here demeaned along each frequency row (i.e., demeaning was performed along the time axis). A burst of post-onset low to high frequency activity is observed in the time-frequency maps spanning a frequency range of ~0.3–20. This increased spectral power shows a 'bimodal' pattern consisting of a low-frequency patch over ~0.3–3 Hz and a high-frequency patch over ~8–20 Hz. In both panels, a negative value on the time-axis means a time point prior to the onset time of the GPFA event.

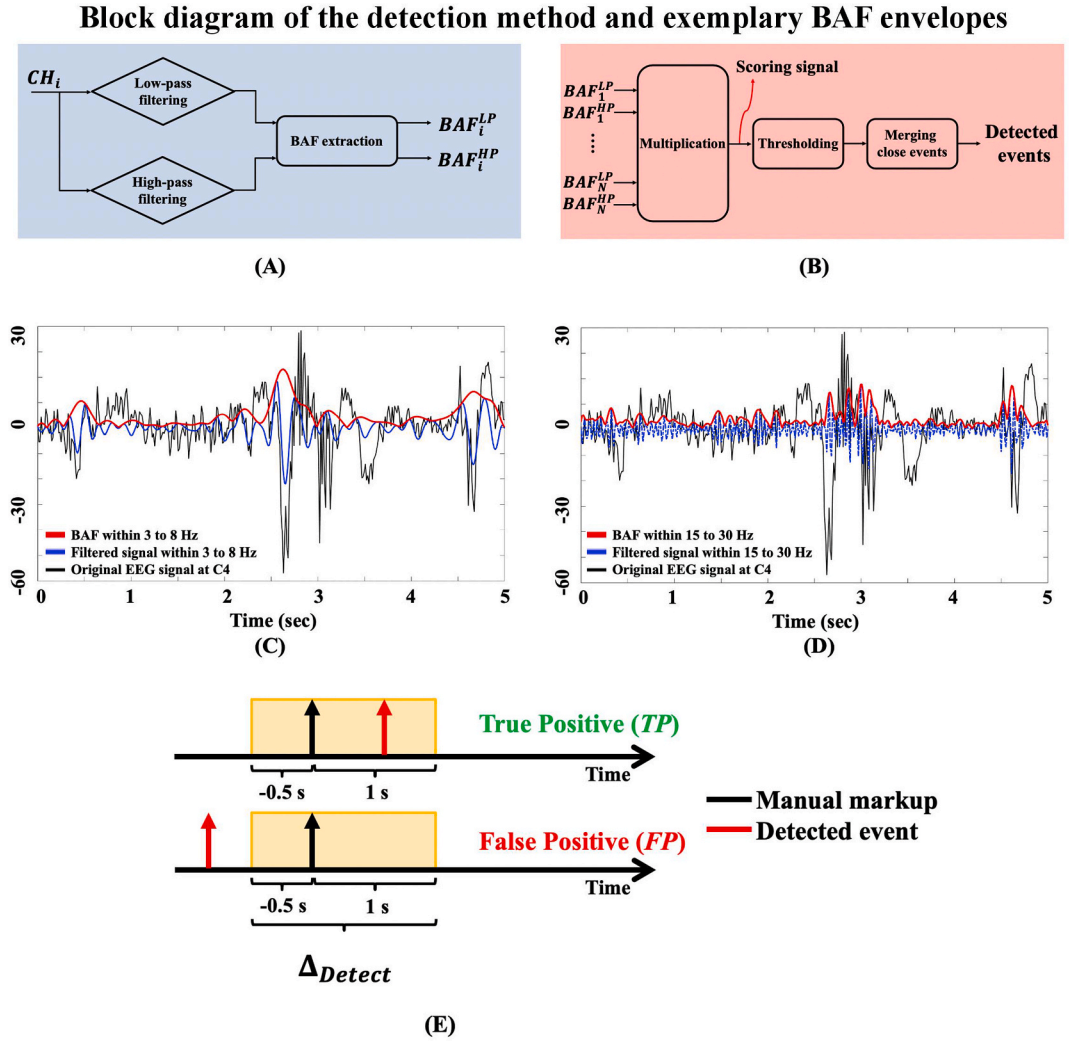

Fig. 3. (A) Schematic of the proposed GPFA detection method at the single electrode channel level. (B) Schematic of the approach at the multi-channel level. (C) Example of a typical band amplitude fluctuation (BAF) envelope for a single EEG channel (C4) within an exemplary frequency band of 3–8 Hz. (D) BAF envelope of the same signal extracted within a higher frequency band of 15–30 Hz. (E) Example of a true positive (TP) and a false positive (FP) event for the adjacency interval Δ_{Detect} of −0.5 to 1 s peri-onset (shaded yellow rectangle). The top line illustrates a true positive event (red arrow) with respect to Δ_{Detect} (black arrow). The bottom line shows a false positive event (red arrow) which is outside of Δ_{Detect} (black arrow).

multi-electrode nature. Fig. 2-A and Fig. 2-B display the average spectrograms of all manually marked GPFAs in a subset of scalp EEG electrodes selected from all LGS patients, calculated over a 6 s time window (−3 to 3 s peri-onset). Spectrograms were defined as the short-time Fourier transform of input signals [22]. The selected EEG electrode in each dataset was chosen as the electrode with maximum spectral power across the frequency range of 8–20 Hz post-event onset. The relevance of this frequency band for GPFA is discussed in section 3.1. In 10 out of 13 datasets, the selected electrode was located in the frontal scalp region. Visual inspection of these time-frequency representations suggested a characteristic pattern of time-frequency changes between the pre- and post-onset intervals in GPFA events. As shown in Fig. 2-A and B, these pre-post onset changes became more apparent after demeaning the time-frequency maps along the time axis (i.e., each frequency row in the maps was converted to have a mean value of zero). We observed a 'bimodal' burst of increased spectral power immediately following GPFA onsets that was most apparent in frontal electrodes and was seen as a simultaneous increase of spectral power in a low frequency range of approximately 0.3–3 Hz and a high frequency range of approximately 8–20 Hz. Based on these observations, we hypothesized a general outline for characterization of GPFA in LGS as follows:

*GPFA is an interictal EEG event associated with a burst of post-onset low to high frequency activity spanning a frequency range of ~0.3-*20 Hz *across multiple, particularly frontal, scalp EEG electrodes. This increased spectral power shows a bimodal pattern consisting of a low frequency patch over ~0.3-*3 Hz *and a higher frequency patch over ~8–*20 Hz s.

To test this hypothesis, we considered three subject-specific parameters for each GPFA event in the time-frequency domain: (*i*) a post-onset low-frequency band (Δ_{LF} in Hz), (*ii*) a post-onset high-frequency band (Δ_{HF} in Hz), and (*iii*) a subset of EEG electrodes with maximal high-frequency information over Δ_{HF}. The peri-onset interval was defined as 1 s before to 2 s after each manually marked IED onset time. To estimate the upper limit of Δ_{LF} in each patient, we divided the mean spectrogram of each GPFA event into pre- and post-onset regions. We then projected the spectrograms along the frequency axis and extracted the upper cut-off frequency of Δ_{LF} where the derivative of spectral difference transited from negative to positive values. To estimate the mid-frequency of Δ_{HF}, we detected the peak of the consistent spectral bumps ranging above Δ_{LF} before and after the EEG onset. We defined the extent of Δ_{HF} as the full width at half maximum of the detected peak. This analysis was performed for each patient separately.

2.4. Validation of the time-frequency feature via automatic IED detection

To validate the utility of the identified time-frequency feature in automatically detected GPFA events, we searched for EEG segments with similar bimodal spectral properties throughout the whole of each patients' in-scanner EEG recording. The rationale here was that if the time-frequency arrangement of GPFA is a reliable and general feature across patients, it should occur during both manually marked GPFA segments as well as GPFA-like segments that were not identified in the original manual markup. Hence our automatic detection procedure is likely to yield both true positives (TPs, events which coincide with the manually marked GPFA segments) as well as false positives (FPs, events which do not coincide with the manually marked GPFA segments but which share similar bimodal spectral behavior). In the following sections, we describe the proposed automatic detection procedure and explain how its true/false positives were quantified.

2.4.1. Automatic detection procedure

Fig. 3-A and Fig. 3-B show block diagrams of the proposed automated event detection strategy at the single-channel and multi-channel levels for a typical EEG dataset. The strategy comprises two main steps: (*i*) analysis of each EEG channel separately (Fig. 3-A), and (*ii*) integration of the channel-wise analyses (Fig. 3-B). At the single-channel level, band-amplitude fluctuations (BAFs) of each channel are extracted using the Hilbert transform. The BAF envelope of a signal $X(t)$ is defined as the absolute value of the analytic associate of its filtered version within a certain frequency band Δf, i.e., $X(t, \Delta f)$ [Omidvarnia et al., 2014]. Mathematically, it is written as:

$$BAF_X(t, \Delta f) = \left| X(t, \Delta f) + i\widehat{X}(t, \Delta f) \right| = \sqrt{X^2(t, \Delta f) + \widehat{X}^2(t, \Delta f)} \quad (1)$$

where $\widehat{X}(t, \Delta f)$ is the Hilbert transform of $X(t, \Delta f)$ and $i = \sqrt{-1}$. Zero-phase band-pass filtering is first performed using a Butterworth filter of order 4 in both forward and backward direction [23]. The BAF of a signal represents its time-varying spectral power within the selected frequency band Δf only. In other words, BAF extraction preserves the spectral content of a GPFA event over time within a selected frequency range while excluding other frequency components that are not of interest.

Fig. 3-C and Fig. 3-D show, for one example dataset, the BAF envelopes for an interictal EEG segment in a typical EEG electrode (here, C4) within a low frequency band of Δf = 3–8 Hz and a high frequency band of Δf = 15–30 Hz. The first step in the proposed GPFA detection approach is to extract two BAF envelopes for each EEG electrode within the pre-defined frequency bands Δ_{LF} and Δ_{HF}. Fig. 3-A illustrates the schematic of this process at C4. For a multi-channel EEG dataset with N_{chan} number of electrodes, the per-channel BAF extraction procedure leads to $2N_{chan}$ BAF envelopes. The per-channel BAF signals are then integrated via multiplication over all channels at each time point (i.e., Hadamard product of the two BAF signals). This step yields what we define here as a *scoring signal* with a duration equal to that of the entire EEG recording (red arrow in Fig. 3-B). For each time-point, the scoring signal indicates the degree to which there is simultaneous high power within both Δ_{LF} and Δ_{HF} frequency bands across the intersection of all EEG channels. An increase in the scoring signal is therefore associated with the potential occurrence of a GPFA-like event with maximal spectral power within these bands. The desired events are detected by selecting supra-threshold time points of the scoring signal after merging adjacent events that are closer than a pre-defined time length, which we refer to as a *merging window* (here, 0.5 s). We used this merging step to avoid detecting multiple events that are too close because such events are more likely to represent a single GPFA burst. Section 2.4.2 explains the choice of our scoring signal threshold.

Given that obtaining Δ_{LF} and Δ_{HF} relies on an initial manual EEG markup, we first estimated these frequency bands using the manually marked datasets of our LGS cohort and then used this estimation as a priori knowledge for our automatic IED detection procedure. In line with the results of the group average time-frequency maps of Fig. 2, we fixed Δ_{LF} to 0.3–3 Hz and Δ_{HF} of 8–20 Hz.

2.4.2. True and false positive rates with reference to manual EEG markup

A key issue regarding the validity of the automatically detected GPFA events is the choice of an appropriate threshold to apply to the scoring signal, above which a potential GPFA-like event is flagged in our automatic detection procedure (Fig. 3-B). To address this, we repeated the detection method for each individual dataset at multiple thresholds from 5% to 95% of the scoring signal amplitude in 5% increments (i.e., 19 thresholds in total per dataset) and counted the number of TPs and FPs at each threshold.

The TP and FP events were defined as follows: we considered each event (either automatically detected event or manually marked GFPA) as a Dirac delta function with zero duration and treated the set of events as a binary pulse train. We deemed an automatically detected event and a manually marked event as similar if their corresponding delta functions were within an *adjacency interval* Δ_{Detect} around the onset time of each manually marked GPFA event. Automatically detected events outside all adjacency intervals were considered to be FP events. Fig. 3-E illustrates examples of TP and FP events with respect to a Δ_{Detect} of −0.5 to 1 s peri-onset interval. This comparison yielded a patient-specific

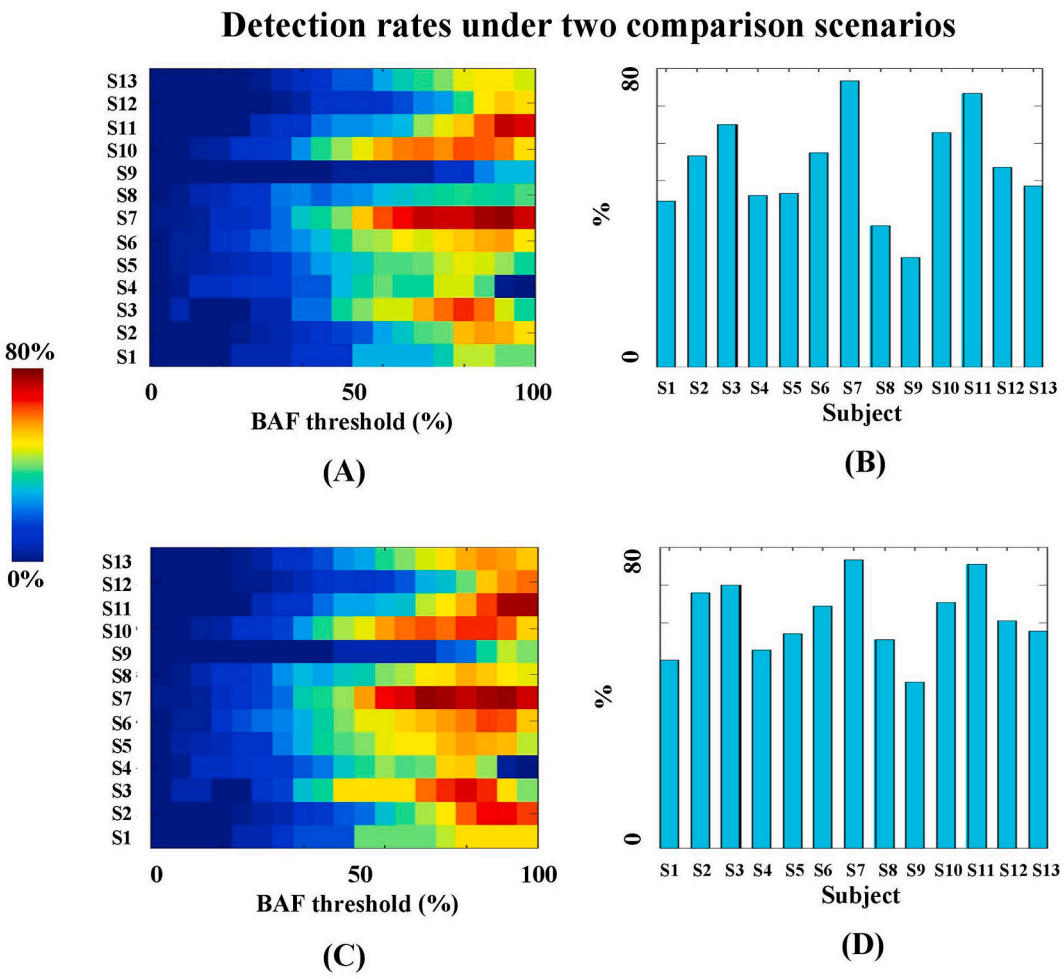

Fig. 4. (A) and (C) Color maps of TPRs using the strict ($\Delta_{Detect} = -0.5$ to 0.5 s) and less strict ($\Delta_{Detect} = -0.5$ to 1 s) comparison procedures with multiple thresholds from 5% to 95% of the scoring signal amplitude in 5% increments. Each row in the maps represents a detection profile for a single patient. (B) and (D): Subject-specific TPRs at the peak of the detection profiles, corresponding to the panels (A) and (C), respectively. Subject IDs (S1, S2, and so on) correspond to Table 1.

spike detection profile for each EEG dataset where the true positive rate (TPR) can be plotted across multiple scoring signal thresholding levels, as illustrated in Fig. 4. The most optimum threshold applied to each scoring signal was obtained as the peak of their spike detection profile, reflecting the threshold at which the TPR was maximal. For each patient, the TPR was defined as:

$$TPR(\Delta_{Detect}) = \frac{N_{TP}(\Delta_{Detect})}{N_{Manual}} \quad (2)$$

where $N_{TP}(\Delta_{Detect})$ is the number of manually marked GPFA events which had at least one corresponding automatically detected event in the proximity of their adjacency interval and N_{Manual} is the total number of manually marked GPFA events (Table 1). The *missing rate* (MR) was defined as:

$$MR(\Delta_{Detect}) = \frac{N_{Missing}(\Delta_{Detect})}{N_{Manual}} \quad (3)$$

where $N_{Missing}(\Delta_{Detect})$ is the number of manually marked events which were missed by the detection algorithm (i.e., $N_{Missing}(\Delta_{Detect}) = N_{Manual} - N_{TP}(\Delta_{Detect})$). In this study, we used two different values for Δ_{Detect}, i.e., −0.5 to 0.5 s (*strict* comparison) and −0.5 to 1 s (*less strict* comparison) peri-onset intervals.

2.4.3. Testing the biological plausibility of 'false positives' via EEG-fMRI analysis

Validation of FPs in the proposed automatic GPFA detection procedure is a non-trivial challenge. Although the FP events do not temporally coincide with the manually marked GPFA events as the gold standard, it is possible that FPs represent genuinely epileptic events that were missed by the human expert due to, for example, markup fatigue (as is likely to occur when manually marking up lengthy EEG recordings) and/or subjective decision-making concerning the threshold at which the manually identified event is deemed to be GPFA or not. Alternatively, some proportion, or even all automatically detected events could be erroneous. In this study, we chose to assess the biological plausibility of FPs by analysing their associated brain hemodynamic response maps using simultaneous fMRI recordings. Our rationale for this analysis was that if FPs are indeed biologically meaningful epileptic events, their brain hemodynamic response maps should resemble the maps derived from manually marked IEDs. A standard event-related general linear modelling (GLM) analysis of concurrent EEG-fMRI was used [24]. We treated the EEG events as a binary sequence of Dirac delta functions and convolved it with a canonical hemodynamic response function, as well as its first-order derivatives with respect to time and space (i.e., a total of three event-related regressors of interest were included per GLM). As nuisance regressors, we included 6 head motion parameters in the GLM, derived from the rigid volume realignment step performed during fMRI pre-processing. For each patient, we performed simultaneous EEG-fMRI analysis using the timing information derived

Table 2
Summary of the estimated low- and high-frequency bands of GPFA for each patient.

ID	Δ_{LF}	Δ_{HF}	EEG channel with maximum Δ_{HF} power
S1	0.3–1.4 Hz	3.3–5.7 Hz	F1
S2	0.3–2.7 Hz	7.6–12.3 Hz	FC5
S3	0.3–1.7 Hz	10.8–12.6 Hz	P5
S4	0.3–3.3 Hz	7.9–12.2 Hz	F3
S5	0.3–2.8 Hz	15.9–17.6 Hz	F5
S6	0.3–3.6 Hz	8.4–13.6 Hz	FP1
S7	0.3–2.6 Hz	6.5–12.8 Hz	FP1
S8	0.3–2.9 Hz	9.8–13 Hz	FC1
S9	0.3–2.7 Hz	7.7–12.3 Hz	FP2
S10	0.3–2.3 Hz	8.7–12.8 Hz	PO6
S11	0.3–2.2 Hz	8.2–13.7 Hz	PO8
S12	0.3–3.3 Hz	10.2–12.8 Hz	F2
S13	0.3–3.3 Hz	9.4–12.4 Hz	FPZ
Mean	**0.3–2.7 Hz**	**8.8–12.6 Hz**	***Frontal electrodes*: 10/13**

from the automatically detected TP and FP events (each of these analyses were performed twice, once for each of the two Δ_{Detect} intervals). In addition, we repeated the analyses using the manually markup GPFA events. This led to 78 separate EEG-fMRI analyses (13 patients $\times$ 3 event types [TP, FP, and manually marked] $\times$ 2 adjacency intervals). For each analysis, a statistical parametric map of hemodynamic signal change was obtained by an *F*-test across the three event regressors of interest.

We hypothesized that if the detected FP events are non-biological, they should lead to spurious statistical parametric maps with low similarity to the maps derived from manual markup. We tested this hypothesis by calculating the pairwise spatial cross-correlation between the *F*-maps associated with the FPs and the *F*-maps associated with manual markup,[6] where a high correlation value indicates that the two maps under consideration are spatially similar. *F*-maps were compared under two circumstances: (*i*) without statistical thresholding and (*ii*) after statistical correction using an uncorrected voxel-wise *p*-value of 0.001 followed by a corrected cluster-wise *p*-value of 0.05 using Gaussian Random Field Theory [25]. All GLM analyses were performed using SPM12 running in MATLAB version R2016a [26].

3. Results

3.1. Estimated frequency intervals

The group-average time-frequency maps of GPFA events in Fig. 2 were observed at the individual level. In other words, a bimodal spectral arrangement was presented in each patient's interictal EEG dataset. The mean low frequency band Δ_{LF} was ~0.3–2.7 Hz and the mean high frequency band was Δ_{HF} = ~8.8–12.6 Hz. The high frequency band Δ_{HF} extended as low as 3.3–5.7 Hz in subject *S1* to 15.9–17.6 Hz in subject *S5*. Across the group, most scalp EEG channels showing the greatest high frequency power over Δ_{HF} were located across frontal and pre-frontal areas (10 of 13 patients). Table 2 summarizes the estimated frequency intervals (i.e., Δ_{LF} and Δ_{HF}) of GPFA events for all patients. Although these frequency intervals are shown in Table 2 for each patient, similar frequency intervals were used for all patients during the automatic detection procedure based on the ensemble means.

3.2. Assessing true positives via comparison with manual markup

Using the mean high/low frequency bands estimated across all patients (see section 3.1), we performed the proposed automatic GPFA detection procedure (Fig. 3) using the fixed frequency bands of Δ_{LF} = 0.3–3 Hz and Δ_{HF} = 8–20 Hz. For each detection, we defined TP and FP events under two scenarios: strict comparison with $H_{Detect} = -0.5$ to 0.5 s peri-onset and less strict comparison with $\Delta_{Detect} = -0.5$ to 1 s peri-onset.

Table 3
Summary of the automatic event detection results for $\boldsymbol{\Delta_{LF}}$ = 0.3–3 Hz and $\boldsymbol{\Delta_{HF}}$ = 8–20 Hz.

$\Delta_{Detect} = -0.5$ *to* 0.5 *sec*			$\Delta_{Detect} = -0.5$ *to* 1 *sec*		
N_{FP}	N_{TP}	*TPR*%	N_{FP}	N_{TP}	*TPR*%
367 ± 179	39 ± 21	53.7 ± 13.6%	412 ± 221	46 ± 26	61.3 ± 9.8%

Table 4
Average spatial correlation between the EEG-fMRI F-maps obtained from manual markup of GPFA events versus all automatically detected events as well as false positive events only. All values are normalized between 0 (minimum spatial similarity) and 1 (full spatial overlap).

$\Delta_{Detect} = -0.5$ *to* 0.5 *sec*	$\Delta_{Detect} = -0.5$ *to* 1 *sec*
Uncorrected *F*-maps of *TP* and *FP* events	
$r = 0.71 \pm 0.13$	$r = 0.71 \pm 0.15$
Uncorrected *F*-maps of *FP* events only	
$r = 0.63 \pm 0.09$	$r = 0.64 \pm 0.12$
Corrected *F*-maps of *TP* and *FP* events	
$r = 0.37 \pm 0.33$	$r = 0.36 \pm 0.37$
Corrected *F*-maps of *FP* events only	
$r = 0.16 \pm 0.19$	$r = 0.22 \pm 0.28$

In general, the number of automatically detected events was considerably higher than the number of manually marked GPFA events. This was reflected in the number of FPs (N_{FP}) compared to the number of TPs (N_{TP}). N_{FP} varied from 367 ± 179 FP detected events for the strict comparison scenario (i.e., $\Delta_{Detect} = -0.5$ to 0.5 s peri-onset) to 412 ± 221 detected events for the less strict comparison scenario (i.e., $\Delta_{Detect} = -0.5$ to 1 s peri-onset), while the range of N_{TP} was 39 ± 21 and 46 ± 26 detected events, respectively.

The detection results are summarized in Table 3. As expected, TPRs associated with the less strict comparison scenario were always higher than the strict comparison scenario (61.3 ± 9.8% versus 53.7 ± 13.6%).

Fig. 4 demonstrates the individual analysis results under the strict and less strict comparison scenarios separately. In the figure, the left column is associated with color-coded spike detection profiles extracted from the LGS datasets. Maximum TPR values associated with the peaks of the spike detection profiles are also plotted as bar plots on the right side.

3.3. Assessing false positives: EEG-fMRI analysis

For each patient, we investigated the spatial correlation between the manual markup *F*-map and its corresponding *F*-map generated from (*i*) *all* automatically detected events (i.e., the combination of TPs and FPs), and (*ii*) FPs only.

Given that the definition of FP and TP events depends on the adjacency interval Δ_{Detect}, we performed the correlation analysis for both $\Delta_{Detect} = -0.5$ to 0.5 s peri-onset and $\Delta_{Detect} = -0.5$ to 1 s peri-onset. For $\Delta_{Detect} = -0.5$ to 0.5 s peri-onset, the average correlation between the manual markup maps and the maps of all detected events was $r = 0.71 \pm 0.13$. This correlation was reduced for the *F*-maps of the FP events to 0.63 ± 0.09 (see Table 4).

We repeated the abovementioned spatial correlation analysis for the statistically corrected *F*-maps at the voxel-wise $p < 0.001$ followed by a cluster-wise $p < 0.05$ correction for multiple comparisons. As Table 4 shows, statistical thresholding to the *F*-maps led of a reduction in the spatial correlation values, presumably due to fewer brain voxels that were present in the *F*-maps after the statistical correction was applied (i.e., $r = 0.37 \pm 0.33$ for the maps of all detected events; and $r = 0.16 \pm 0.19$ for the maps associated with the FP events only, all

[6] Spatial cross-correlation was calculated using the FSL command *fslcc*. See https://fsl.fmrib.ox.ac.uk/fsl/fslwiki/Fslutils for more details.

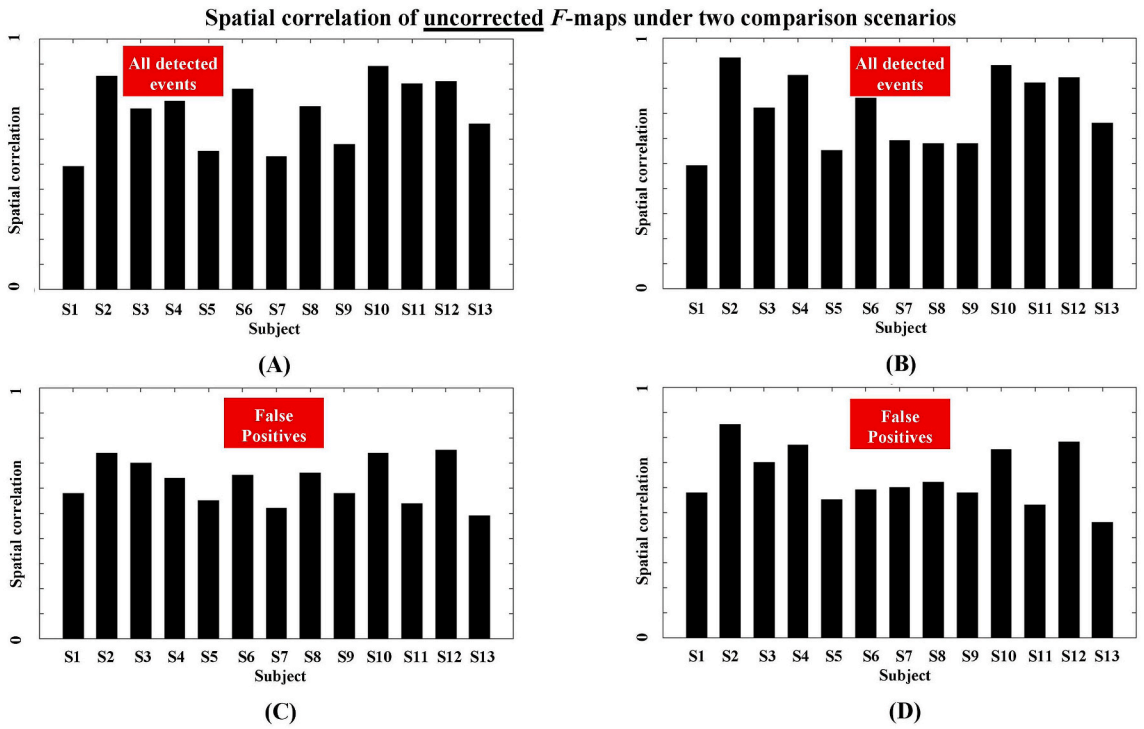

Fig. 5. Spatial correlation between the uncorrected F-maps of manual markup and automatically detected events for the strict comparison scenario or $\Delta_{Detect} = -0.5$ to 0.5 s peri-onset (panels A and C on the left) and the less strict comparison scenario or $\Delta_{Detect} = -0.5$ to 1 s peri-onset (panels B and D on the right). Top row panels (A and B) show correlation values with the F-maps of all detected events. Bottom row panels (C and D) show correlation with the F-maps of the false positives only. Subject IDs correspond to Table 1.

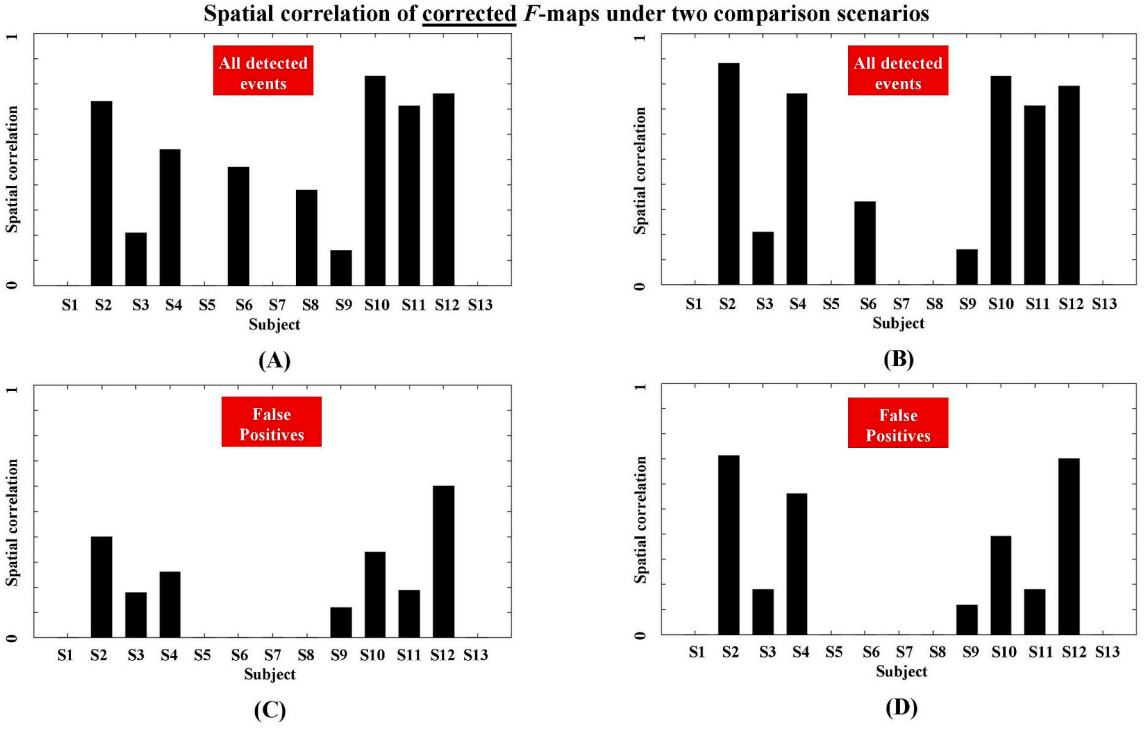

Fig. 6. Similar caption as for Fig. 5, but for the corrected F-maps.

obtained at $\Delta_{Detect} = -0.5$ to 0.5 s peri-onset). As Table 4 suggests, changing Δ_{Detect} to -0.5 to 1 s peri-onset did not have a strong impact on the spatial correlation values, similar to what was observed for the uncorrected *F*-maps.

Fig. 5 and Fig. 6 demonstrate the subject-specific spatial correlation values as bar plots, before and after statistical correction of the *F*-maps. Examples of the GPFA *F*-maps with high correlation between automatically detected events and manual markup are illustrated in Fig. 7.

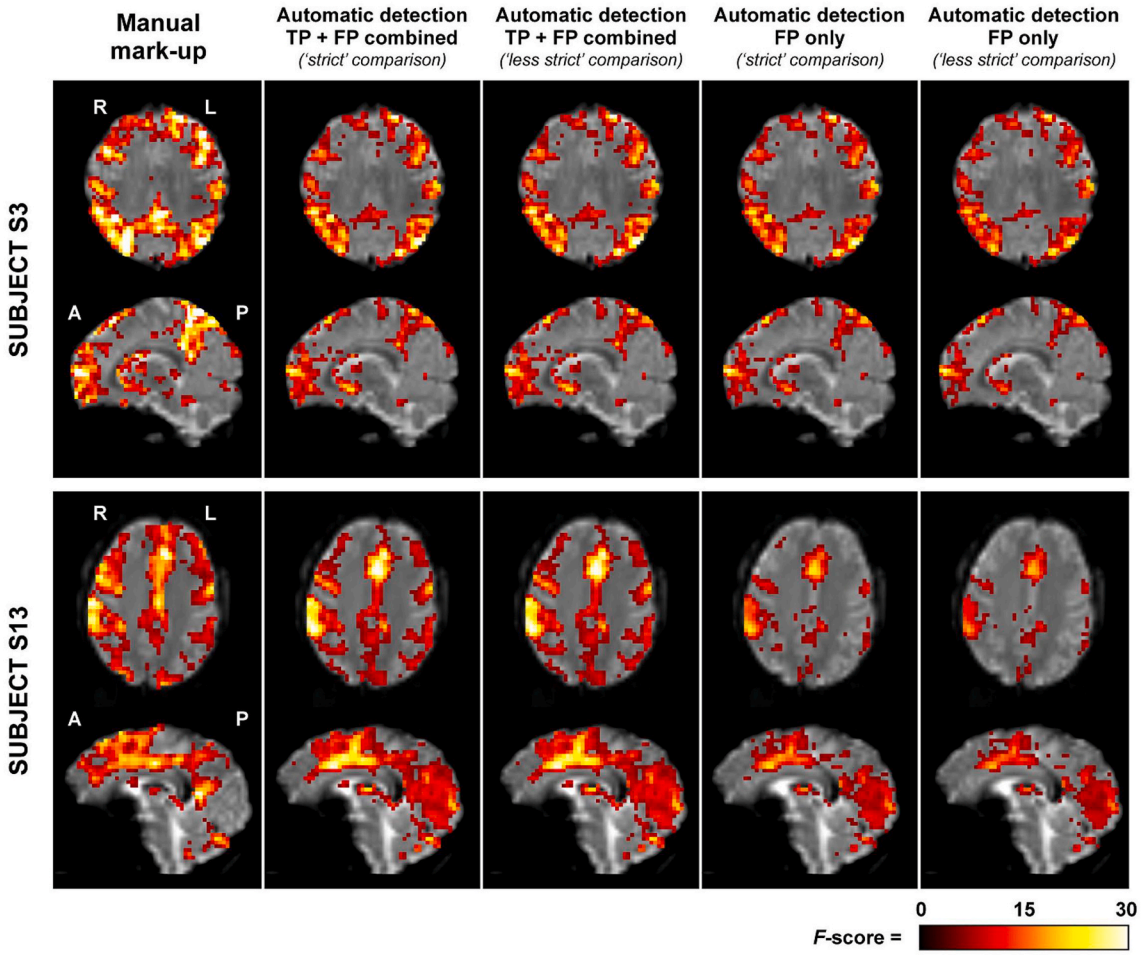

Fig. 7. F-maps of EEG-fMRI analysis based on the timing of GPFA events for subjects S3 and S13 as two exemplary cases with high spatial agreement between automatic GPFA detection and manual markup. Acronyms: TP = True Positive, FP = False Positive.

4. Discussion

Our study reveals a bimodal time-frequency feature associated with GPFA, a generalized IED type characteristic of the interictal EEG in LGS. The proposed automatic IED detection approach can highlight interictal EEG segments with similar time-frequency information and can thus identify EEG events that are likely similar to manually marked GPFA. The validity of this approach was examined by spatial correlation analysis showing that EEG-fMRI brain maps derived from 'false positives' only (i.e., automatically detected EEG events which were not originally marked up manually) are comparable to those derived from manual IED markup.

Bimodality in the spectral content of GPFA implies that these IEDs carry *nested* high frequency oscillations that are superimposed upon slower fluctuations occurring during peri-onset intervals. This feature spans a low-frequency band of ~0.3–3 Hz, and a high-frequency band of ~8–12 Hz which in some patients may extend up to 20 Hz. Scalp EEG electrodes associated with frontal and pre-frontal areas tend to show the greatest high frequency power in the GPFA events, consistent with the earlier work suggesting a key role of frontal cortex in driving GPFA [20].

These results build on our previous study [27] which developed an automatic detection method for focal IEDs (i.e., events which are concentrated in time and space) in focal epilepsy patients. In contrast to this previous study, which focussed on detecting epileptic discharges with uniform morphology over time at a single EEG channel, automatic detection of GPFA presents additional unique challenges: (*i*) the precise onset time of generalized discharges can be difficult to define with respect to the EEG background; (*ii*) even within a single patient, there is often variability in morphology and frequency from one discharge to the next, or over the course of a discharge train; and (*iii*) discharges can be spatially variable and show propagation over multiple EEG channels. Our current work aimed to address these challenges by inspecting generalized IEDs across multiple EEG channels and characterizing their joint temporo-spectral properties.

Time-frequency characterization of manually marked GPFA events suggests that their bimodal spectral characteristic is replicable over patients. However, the specific frequency bands of interest may vary considerably across individuals. We assessed the robustness of this time-frequency feature via an automatic search for similar dynamics throughout patients' interictal EEG recordings. We hypothesized that if this EEG signal feature is reproducible across patients, it should be able to highlight both manually marked GPFA as well as GPFA-like events that were missed in the manual markup. Across patients, the agreement between manually marked IEDs and automatically detected IEDs varied from ~40% to ~80%. Even though the number of false positives was generally higher than the number of manually marked IEDs (see the N_{FP} columns in Table 3), the associated *F*-maps generated by EEG-fMRI analysis were spatially similar to the corresponding *F*-maps derived from manual markup. This spatial overlap was above $r = 0.5$ in most analyses, when the zero-thresholded *F*-maps were compared. It was also similar for the *F*-maps extracted from false positives only and the maps generated based on the combination of true and false positives. Spatial overlap was reduced after statistical correction of the EEG-fMRI *F*-maps. This was also reflected in the group-mean correlation values of GPFA in

Table 4. Less strict comparison of the automatically detected events with reference to manual markup (i.e., post-onset interval of 1 s in contrast to 0.5 s in Δ_{Detect}) had negligible impact on the spatial correlation values of the *F*-maps. This finding suggests that EEG-fMRI analysis of GPFA is relatively robust to minor variability in the precise EEG onset of IEDs (either manually marked or automatically detected), likely due to the comparatively slow event-related hemodynamic response measured by fMRI.

The proposed GPFA detection method in this study relies on an initial manual markup of EEG, because the time-frequency characteristics of GPFA (i.e., the two frequency bands Δ_{HF} and Δ_{LF}) have to be customized and estimated for each subject a priori. The main idea behind the practical implementation of the proposed analysis framework is to manually mark a few numbers of GPFA events by an EEG expert, compute their mean spectrogram, and estimate the associated Δ_{HF} and Δ_{LF}. Although this step has to be repeated for each subject, it is considerably more convenient than a complete manual markup, in particular, for long EEG recordings. This is because manual markup of a small number of GPFA events would be far easier, more accurate, and much faster than going through the entire (often long-length) EEG recordings and trying to spot all GPFA events visually. The promising detection results may also facilitate faster simultaneous EEG-fMRI analysis in LGS. This is important because it may assist with pre-surgical planning of LGS, for example, in guiding optimal thalamic stimulation targets in patients undergoing deep brain stimulation [28] or identifying potentially resectable epileptogenic cortical lesions.

5. Conclusion

GPFA shows a characteristic bimodal time-frequency feature that can be automatically detected in patients with LGS. The spectral extent of this feature may vary across patients, but it is mainly presented in the time-frequency domain as two high power frequency bands of ~0.3–3 Hz and ~8–13 Hz. The utility of this time-frequency feature is demonstrated by EEG-fMRI analysis of automatically detected GPFA events, which recapitulates the brain network patterns we have previously shown to underlie manually marked generalized IEDs in LGS. Fast and easy implementation of the proposed analysis framework on long-length EEG recordings may pave the way for developing objective, accurate, efficient and low-cost software packages for automatic GPFA detection which can be used in real-life environments, research applications, and clinical settings.

CRediT authorship contribution statement

Amir Omidvarnia: Conceptualization, Methodology, Software, Formal analysis, Validation, Writing – original draft. **Aaron E.L. Warren:** Conceptualization, Methodology, Data curation, Validation, Writing – review & editing. **Linda J. Dalic:** Conceptualization, Data curation, Resources, Validation, Writing – review & editing. **Mangor Pedersen:** Conceptualization, Methodology, Validation, Writing – review & editing. **Graeme Jackson:** Conceptualization, Resources, Writing – review & editing, Supervision.

Declaration of competing interest

None of the authors have potential conflicts of interest to be disclosed.

Acknowledgement

A.O. acknowledges financial support through the Eurotech Postdoc Programme, co-funded by the European Commission under its framework programme Horizon 2020 (Grant Agreement number 754462). This work was supported by the National Health and Medical Research Council (NHMRC) of Australia (program grant 628952). G.J. was supported by an NHMRC practitioner fellowship (1060312). A.E.L.W was supported by a post-doctoral research fellowship from the Lennox-Gastaut syndrome Foundation (www.lgsfoundation.org). The Florey Institute of Neuroscience and Mental Health acknowledges the strong support from the Victorian Government and in particular the funding from the Operational Infrastructure Support Grant. The authors acknowledge the facilities, and the scientific and technical assistance of the National Imaging Facility at the Florey Node. We thank Dr. Magdalena Kowalczyc, Dr. John Archer and Dr. Simon Harvey for assistance with patient recruitment, EEG-fMRI data acquisition and useful discussion.

References

[1] J.S. Archer, A.E.L. Warren, M.R. Stagnitti, R.A.J. Masterton, D.F. Abbott, G. D. Jackson, Lennox-Gastaut syndrome and phenotype: secondary network epilepsies, Epilepsia 55 (8) (Aug. 2014) 1245–1254, https://doi.org/10.1111/epi.12682.

[2] U. Intusoma, et al., Tonic seizures of Lennox-Gastaut syndrome: periictal single-photon emission computed tomography suggests a corticopontine network, Epilepsia 54 (12) (Dec. 2013) 2151–2157, https://doi.org/10.1111/epi.12398.

[3] P. Halász, J. Janszky, G. Barcs, A. Szucs, Generalised paroxysmal fast activity (GPFA) is not always a sign of malignant epileptic encephalopathy, Seizure 13 (4) (Jun. 2004) 270–276, https://doi.org/10.1016/S1059-1311(03)00145-6.

[4] A.E.L. Warren, D.F. Abbott, D.N. Vaughan, G.D. Jackson, J.S. Archer, Abnormal cognitive network interactions in Lennox-Gastaut syndrome: a potential mechanism of epileptic encephalopathy, Epilepsia 57 (5) (May 2016) 812–822, https://doi.org/10.1111/epi.13342.

[5] F.E.A. El-samie, T.N. Alotaiby, M.I. Khalid, S.A. Alshebeili, S.A. Aldosari, A review of EEG and MEG epileptic spike detection algorithms, IEEE Access 6 (2018) 60673–60688, https://doi.org/10.1109/access.2018.2875487.

[6] M. Feucht, et al., Simultaneous spike detection and topographic classification in pediatric surface EEGs, Neuroreport 8 (9) (Jul. 1997) 2193–2197.

[7] P. Valenti, E. Cazamajou, M. Scarpettini, A. Aizemberg, W. Silva, S. Kochen, Automatic detection of interictal spikes using data mining models, J. Neurosci. Methods 150 (1) (Jan. 2006) 105–110, https://doi.org/10.1016/j.jneumeth.2005.06.005.

[8] L. Logesparan, E. Rodriguez–Villegas, ", A novel phase congruency based algorithm for online data reduction in ambulatory EEG systems, IEEE Trans. Biomed. Eng. 58 (10) (Oct. 2011) 2825–2834, https://doi.org/10.1109/TBME.2011.2160639.

[9] R.R. Sharma, R.B. Pachori, "Time–frequency representation using IEVDHM–HT with application to classification of epileptic EEG signals, IET Sci. Meas. Technol. 12 (1) (2018) 72–82, https://doi.org/10.1049/iet-smt.2017.0058.

[10] D. Karacor, S. Nazlibilek, M.H. Sazli, E.S. Akarsu, Discrete lissajous figures and applications, IEEE Trans. Instrum. Meas. 63 (12) (Dec. 2014) 2963–2972, https://doi.org/10.1109/TIM.2014.2318891.

[11] S.S. Lodder, J. Askamp, M.J.A.M. van Putten, Inter-ictal spike detection using a database of smart templates, Clin. Neurophysiol. 124 (12) (Dec. 2013) 2328–2335, https://doi.org/10.1016/j.clinph.2013.05.019.

[12] M. Mohammadi, et al., Asymmetrical generalized paroxysmal fast activities in children with intractable localization-related epilepsy, Brain Dev. 37 (1) (Jan. 2015) 59–65, https://doi.org/10.1016/j.braindev.2014.03.006.

[13] J. Gotman, J.R. Ives, P. Gloor, Automatic recognition of inter-ictal epileptic activity in prolonged EEG recordings, Electroencephalogr. Clin. Neurophysiol. 46 (5) (May 1979) 510–520, https://doi.org/10.1016/0013-4694(79)90004-X.

[14] J. Gotman, P. Gloor, "Automatic recognition and quantification of interictal epileptic activity in the human scalp EEG," *Electroencephalogr*, Clin. Neurophysiol. 41 (5) (Nov. 1976) 513–529, https://doi.org/10.1016/0013-4694(76)90063-8.

[15] R.R. Sharma, P. Varshney, R.B. Pachori, S.K. Vishvakarma, Automated system for epileptic EEG detection using iterative filtering, IEEE Sens. Lett. 2 (4) (Dec. 2018) 1–4, https://doi.org/10.1109/LSENS.2018.2882622.

[16] J. Bourien, J.J. Bellanger, F. Bartolomei, P. Chauvel, F. Wendling, Mining reproducible activation patterns in epileptic intracerebral EEG signals: application to interictal activity, IEEE Trans. Biomed. Eng. 51 (2) (Feb. 2004) 304–315, https://doi.org/10.1109/TBME.2003.820397.

[17] A. Ossadtchi, S. Baillet, J.C. Mosher, D. Thyerlei, W. Sutherling, R.M. Leahy, Automated interictal spike detection and source localization in magnetoencephalography using independent components analysis and spatio-temporal clustering, Clin. Neurophysiol. 115 (3) (Mar. 2004) 508–522, https://doi.org/10.1016/j.clinph.2003.10.036.

[18] J.H. Cross, S. Auvin, M. Falip, P. Striano, A. Arzimanoglou, "Expert opinion on the management of lennox–gastaut syndrome: treatment algorithms and practical considerations, Front. Neurol. 8 (2017), https://doi.org/10.3389/fneur.2017.00505.

[19] A. Arzimanoglou, et al., Lennox-Gastaut syndrome: a consensus approach on diagnosis, assessment, management, and trial methodology, Lancet Neurol. 8 (1) (Jan. 2009) 82–93, https://doi.org/10.1016/S1474-4422(08)70292-8.

[20] A.E.L. Warren, et al., The epileptic network of Lennox-Gastaut syndrome: cortically driven and reproducible across age, Neurology (Jun. 2019), https://doi.org/10.1212/WNL.0000000000007775.

[21] A. Delorme, S. Makeig, EEGLAB: an open source toolbox for analysis of single-trial EEG dynamics including independent component analysis, J. Neurosci. Methods 134 (1) (Mar. 2004) 9–21, https://doi.org/10.1016/j.jneumeth.2003.10.009.
[22] A.V. Oppenheim, R.W. Schafer, J.R. Buck, Discrete-time Signal Processing, second ed., Prentice-Hall, Inc., USA, 1999.
[23] F. Gustafsson, Determining the initial states in forward-backward filtering, IEEE Trans. Signal Process. 44 (4) (Apr. 1996) 988–992, https://doi.org/10.1109/78.492552.
[24] C.G. Bénar, et al., The BOLD response to interictal epileptiform discharges, Neuroimage 17 (3) (Nov. 2002) 1182–1192.
[25] K.J. Friston, K.J. Worsley, R.S. Frackowiak, J.C. Mazziotta, A.C. Evans, Assessing the significance of focal activations using their spatial extent, Hum. Brain Mapp. 1 (3) (1994) 210–220, https://doi.org/10.1002/hbm.460010306.
[26] D. Veltman, C. Hutton, SPM99 Manual, May 2001 [Online]. Available: http://www.fil.ion.ucl.ac.uk/spm/doc/manual/manual.pdf.
[27] A. Omidvarnia, M.A. Kowalczyk, M. Pedersen, G.D. Jackson, Towards fast and reliable simultaneous EEG-fMRI analysis of epilepsy with automatic spike detection, Clin. Neurophysiol. (Dec. 2018), https://doi.org/10.1016/j.clinph.2018.11.024.
[28] J.S. Archer, A.E.L. Warren, G.D. Jackson, D.F. Abbott, "Conceptualizing lennox–gastaut syndrome as a secondary network epilepsy, Front. Neurol. 5 (Oct. 2014), https://doi.org/10.3389/fneur.2014.00225.